Tribology International 60 (2013) 127–135

Contents lists available at SciVerse ScienceDirect

Tribology International

journal homepage: www.elsevier.com/locate/triboint

Tribological properties of nanostructured DLC coatings deposited by C_{60} ion beam

Oleksiy V. Penkov [a], Volodymyr E. Pukha [b], Evgeniy N. Zubarev [b], Shin-Sung Yoo [a,c], Dae-Eun Kim [a,c,*]

[a] Center for Nano-Wear, Yonsei University, Seoul 120-749, Republic of Korea
[b] National Technical University "KhPI", 61002 Kharkov, Ukraine
[c] Department of Mechanical Engineering, Yonsei University, Seoul 120-749, Republic of Korea

ARTICLE INFO

Article history:
Received 13 August 2012
Received in revised form
5 November 2012
Accepted 8 November 2012
Available online 23 November 2012

Keywords:
C_{60} ion beam
Coating
Nano-composite
DLC

ABSTRACT

The frictional and wear characteristics of nanostructured DLC films were investigated. The coatings were deposited on silicon substrates by irradiation of a mass-separated C_{60} ion beam with 5 keV of energy and a deposition temperature ranging from 100 to 450 °C. The effects of deposition temperature on the surface morphology, nano-structure, mechanical properties and tribological characteristics of the coatings were assessed. Results showed that deposition temperature strongly affects the nanostructure and surface morphology of the coatings. Coatings deposited at temperatures exceeding 350–400 °C exhibited an increase in surface roughness as well as compressive stress due to the formation of graphite, which led to a significant increase in the friction coefficient and wear rate. Coatings deposited at 300 °C showed the best tribological properties.

1. Introduction

The use of nano-structured thin solid films has been steadily increasing in various fields of science and technology, such as magnetic media technology, high-density information storage systems, and micro- and nano-electromechanical systems (MEMS and NEMS) [1]. Many of these applications involve moving parts, making mechanical reliability a key issue [2]. Because of the small size of components in these micro-systems, the friction and wear phenomena in combination with the relatively large surface forces determine the reliability of the devices. Various methods have been developed to solve the problem of reliability including the deposition of a thin layer of soft metal such as silver, gold or aluminum [3], composite coatings based on carbon nanotubes (CNT) [4], organic compounds such as self-assembled monolayers (SAMs) [5], diamond-like carbon films (DLC) [6,7]and DLC-based multilayer coatings [8,9]

DLC films are unique due to high hardness, low friction coefficient, IR transparency, chemical inertness, biocompatibility, impermeability and anti-sticking characteristics [6,10] The disadvantages of DLC films are that they have a high level of internal compressive stress [11], poor adhesion and ambient conditions (humidity) have a strong influence on their tribological properties [12]. High humidity can significantly increase the friction of hydrogenated DLC coatings in ambient conditions [13]. In case of hydrogen-free coatings, low friction and wear can be achieved in both vacuum and ambient conditions. The use of alternative deposition methods such as C_{60} ion beam deposition [14] minimizes these drawbacks due to the formation of nano-composite structures with several interesting features. Gaber et al. was the first to deposit nano-composite carbon-DLC coatings [14]. The coatings were deposited using C_{60} ions with 1 keV of energy at RT. It was found that when the deposition temperature was increased up to 730 °C, the coatings consisted of graphitic nano-crystallites embedded with amorphous carbon and preferentially oriented with the *c*-axis parallel to the surface. As the deposition temperature increased, the size of the crystallites increased together with a decrease in the percentage of sp^3 carbon. Elevating the C_{60} ion energy up to 5 keV led to the formation of similar graphite nano-crystals but at lower deposition temperatures (about 400 °C) [15,16]. Although there are several publications examining the effects of deposition parameters and mechanical properties of nano-composite carbon coatings, their tribological properties and mechanisms of wear have not been studied.

In this study, the effects of deposition parameters on the nanostructure, surface morphology and tribological properties of nano-composite carbon coatings deposited by a C_{60} ion gun were investigated. The methods used for specimen fabrication and the experimental details are described in the following sections.

2. Experimental details

2.1. Synthesis of carbon nano-composite coatings and characterization

Carbon nano-composite coatings were deposited by bombardment of a (100) silicon substrate with high-energy fullerene ions

* Corresponding author at: Department of Mechanical Engineering, Yonsei University, Seoul 120-749, Republic of Korea
E-mail address: kimde@yonsei.ac.kr (D.-E. Kim).

0301-679X/$ - see front matter © 2012 Elsevier Ltd. All rights reserved.
http://dx.doi.org/10.1016/j.triboint.2012.11.011

[15,16]. Fig. 1 presents a schematic view of the deposition setup. Deposition was carried out in a vacuum chamber at a pressure of $\sim 1 \times 10^{-4}$ Pa. The ion beam was generated by a source with a saddle-shaped electric field. The ion beam from the source chamber was collimated and directed to a magnetic mass-separator. The maximum ion current density in the deposition area amounted to 0.02 mA/cm^2. The coatings were deposited at a normal angle of incidence. To achieve spatial uniformity of the coatings, the substrate holder was moved back and forth through the ion beam during deposition. The volume charge of the beam was neutralized by a low-energy electron gun positioned near the substrate. The energy of electrons used for neutralization did not exceed 30 eV. The energy distribution in the ion beam (Fig. 2) was calculated using the data acquired with a multi-grid probe [17].

A C_{60} vapor was used as the working medium. C_{60}-fullerene powder with a purity of 99.5% (NeoTechProducts, Saint Petersburg, Russia) was used as the source material. The fullerene powder was purified by vacuum distillation before use. To prevent the C_{60} from condensing onto the inner walls, the ion source was heated up to 400 °C.

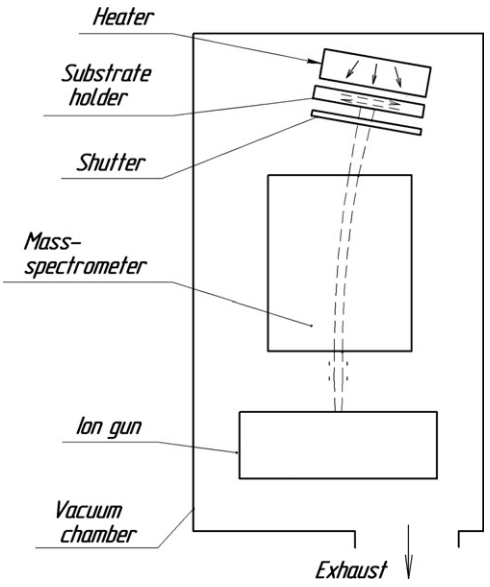

Fig. 1. Schematic of the deposition setup.

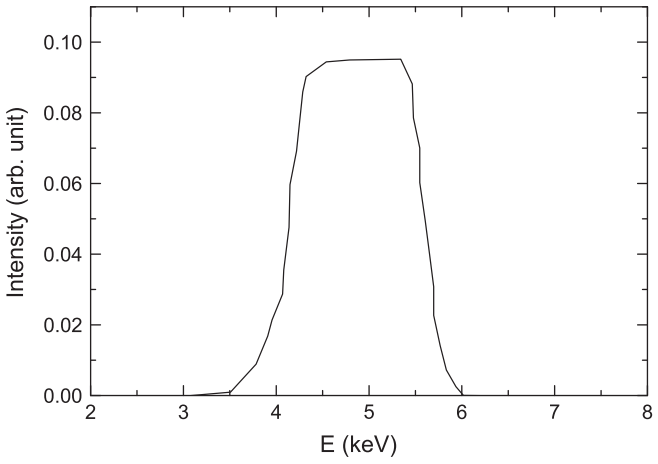

Fig. 2. Energy distribution of C_{60} ions after traveling through the magnetic mass separator.

Transmission electron microscopy (TEM) and small aperture electron diffraction (SAED) analyses were conducted using a PEM-125 K transmission electron microscope with a 0.2 nm point-to-point resolution. Samples were prepared for TEM analysis after deposition by chemical etching of the silicone substrate in an acidic mixture of HF:HNO_3 = 1:10. The free films were then washed in deionized water and placed onto a copper grid.

The fringes of equal thickness (FET) method was used to measure the thickness of the coatings. A sharp step down to the substrate was made with a silicon mask by deposition of Ag onto both the film and substrate [18]. The nano-hardness and elastic modulus were measured using a MTS G200 nano-indenter with a Berkovich diamond tip ($R < 20$ nm) by the continuous depth-sensing indentation technique, which allows the modulus and hardness to be obtained as functions of penetration depth. Only 1-μm-thick coatings were used in the measurements. The hardness values were taken for the indentation depth equivalent to ~10% (100–120 nm) of the film thickness. The average values of six measurements were obtained.

The structure, chemical composition and surface morphology of the coatings were investigated using a scanning electron microscope (SEM; Jeol 6210) equipped with an energy-dispersive X-ray spectroscopy (EDS; OXFORD INCA Energy) system, Raman spectroscopy (Raman; LabRam Aramis) at wavelength of 514.532 nm, and an atomic force microscope (AFM; Seiko SPA400), respectively. The AFM images were measured in contact mode at a 1 Hz sampling rate and a resolution of 512 lines with 512 pixels per line. A silicon tip with a radius of 10 nm was used.

The biaxial film stress was calculated from the curvature radius of the Si (100) substrate using the modified Stoney's equation expressed as follows [19]:

$$\sigma = \frac{E}{(1-\mu)} \frac{h^2}{6Rt}, \quad (1)$$

where σ is the stress in the coating, E is the Young's modulus of the substrate, h is the thickness of the substrate, t is the thickness of the coating, R is the curvature radius of the substrate after film deposition and μ is the Poisson's ratio of the substrate. For measurement of stress in the coating, coatings were deposited on Si substrates with dimensions of 1×10 mm^2. Identical deposition process used to prepare the coatings for the friction and wear tests was used to prepare the coating specimens for stress measurement. The long side of specimen was parallel to ⟨100⟩ orientation of the Si substrate. Young's modulus and Poisson's ratio for the Si (100) were 130 GPa and 0.28, respectively [20].

2.2. Tribological investigation of the coatings

The tribological behavior of the coatings was investigated using a commercial reciprocating tribo-tester (CETR UMT-2). Tests were performed under ambient conditions at a temperature of ~24 °C and a relative humidity of 45–55% under dry sliding conditions. All of the tests were performed under a relatively low applied normal load of 400 mN at a sliding speed of 10 mm/s with a 2 mm stroke, which resulted in the reciprocating frequency of 2.5 Hz. The corresponding contact pressure estimated from the Hertzian equation [21] was approximately 1.2 GPa. Silicon nitride balls with a diameter of 1 mm were used as pins. At least three sliding tests were repeated for each experimental condition, and a new pin was used for each experiment. The total number of cycles ranged from 300 to 45,000, depending on the wear resistance of each specimen. All of the experiments were performed in a class 100 clean room. The amount of wear was calculated from the 2-D cross-sectional profile of the wear track obtained by the AFM.

3. Results and discussion

3.1. Nano-structure of the coatings

The structures of the carbon coatings deposited using a C_{60} ion beam at deposition temperatures of 100 °C and below were amorphous. TEM images of these amorphous coatings had a typical type of a contrast formed by a defocused objective lens. A SAED pattern (Fig. 3a) of the coating demonstrated a halo with characteristic maximums of amorphous carbon. These maximums corresponded to an interplanar spacing of 0.112 and 0.207 nm [22]. Increasing the deposition temperature up to 200 °C led to the formation of an additional halo near the primary beam on the SAED pattern (Fig. 3b). This was the beginning of the formation of sp^2 layered nanostructures consisting of basic graphite layers [23]. At deposition temperatures of 300–350 °C this additional halo was transformed to a diffuse ring. This ring corresponded to an interplanar spacing of 0.32 nm that was close to the (002) spacing of graphite (0.336 nm [24]). A further increase in the deposition temperatures led to the transfer of diffraction intensity to the ring corresponding to diffraction of the (002) plane, and another ring corresponding to the (004) graphite plane appeared (Fig. 3c). These changes in the diffraction patterns confirmed the formation of a graphite phase in the coating at deposition temperatures higher than 200 °C. In addition, the grain size of the graphite nano-crystals increased in conjunction with an increase in deposition temperature.

Bright-field TEM images of coatings deposited at 200–400 °C (Fig. 4) showed additional small areas of 1–2 nm (indicated by arrow in Fig. 4) in which a stripe contrast appeared. The distance between stripes was greater than 0.3 nm. Graphene planes of the graphite crystals were also observed. Dark-field images were obtained from the (002) graphite refraction areas restricted by a 30 μm aperture diaphragm. The corresponding refraction areas

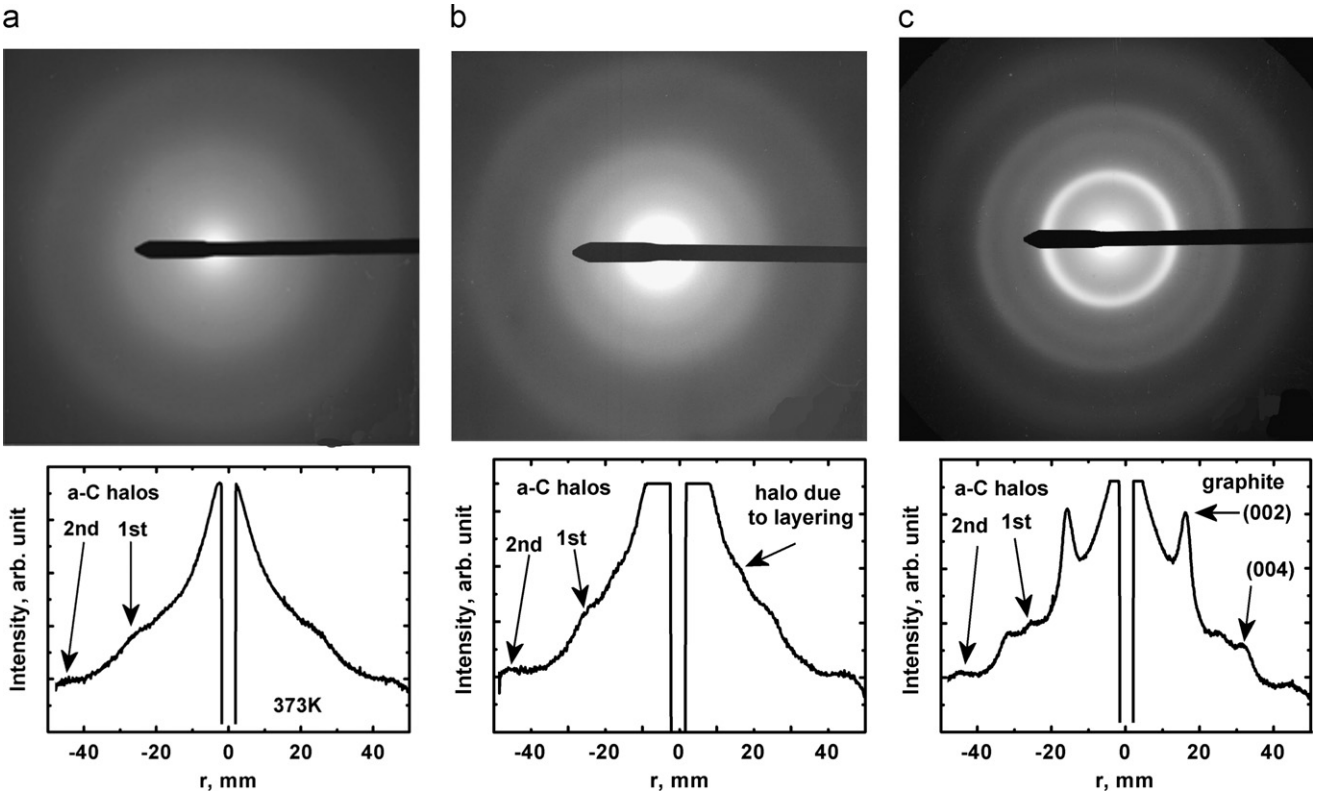

Fig. 3. SAED patterns and photometric measurements of coatings deposited at (a) 100 °C, (b) 200 °C and (c) 400 °C.

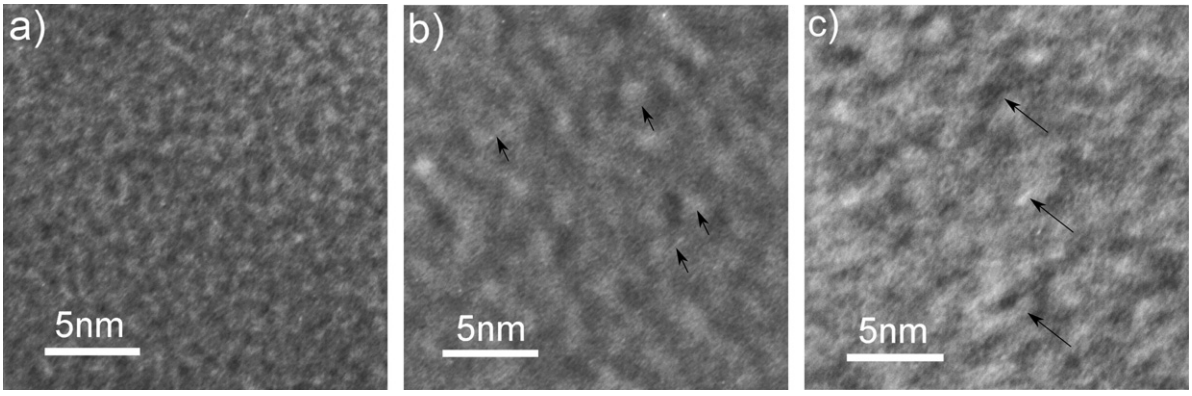

Fig. 4. Bright-field TEM images of coatings deposited at (a) 100 °C, (b) 200 °C and (c) 400 °C (arrows indicate the areas of stripe contrast).

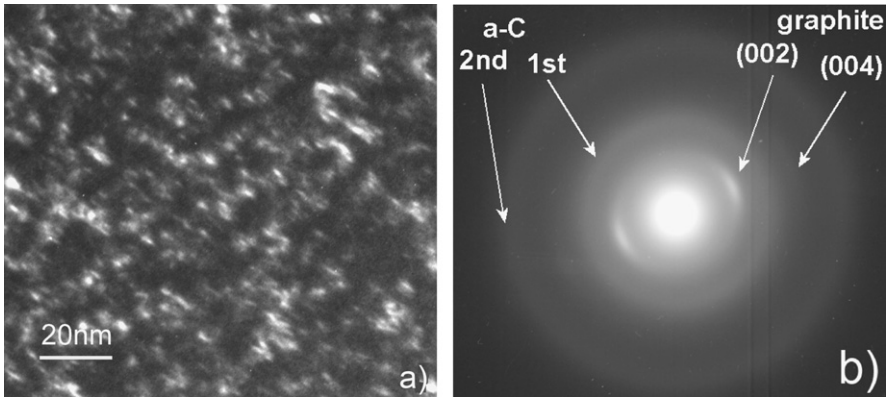

Fig. 5. (a) Dark-field TEM image and (b) 20° tilted SAED of the coating deposited at 400 °C.

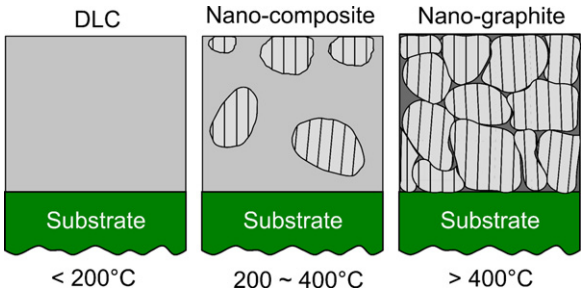

Fig. 6. Schematic of the nano-structure of the coatings depending on the deposition temperature.

were adjusted on the optical axis of the microscope by a deflecting system. Very bright contrast elements with a characteristic size of 1–2 nm were evident on the dark-field images (Ts=400 °C, Fig. 5a). These diffraction elements were identified as graphite nano-crystals.

A decrease in interplanar spacing in the graphite nano-crystals was observed on the SAED patterns for all the coatings having reflections corresponding to graphite base planes. The peak of the (002) reflection corresponded to a spacing of 0.32 nm and it did not shift at deposition temperatures in the range of 300–500 °C. It was shown in [23] that coatings deposited at Ts ~400 °C and ion energy of 5 keV have a nano-composite structure and the decrease in the interplanar spaces is caused by interphase stresses. Compressed graphite nano-crystals were included in a diamond-like matrix with a high concentration of sp^3 bonds, and this matrix was in a tensile state.

The coatings also exhibited a characteristic texture at high deposition temperatures. After tilting the specimen 20° inside the TEM column, the rings corresponding to graphite nano-crystals were transformed to arcs (Fig. 5b). This indicates that the preferred orientation of the graphite nano-crystals is when the normal to the (002) planes is parallel to the surface of the substrate. This kind of texture was observed at all deposition temperatures at which nano-crystals existed. Fig. 6 shows the schematics of the structure of coatings depending on the deposition temperature.

The characteristics of the coatings were further analyzed by Raman spectroscopy at a wavelength of 514 nm. The Raman spectra with respect to the deposition temperature are shown in Fig. 7. As can been seen from the figure, D and G peaks are present on all Raman spectra which is indicative of a DLC coating. Variation of the deposition temperature led to a shift in the G-peak position. Initially, it shifted from 1568 to 1585 cm^{-1} as the deposition temperature increased from 100 to 300 °C. At 400 °C, G-peak shifted back to 1564 and its position remained the same at 450 °C. This shift of G-peak position could be attributed to the structural changes in the coatings, especially to the variation of sp^3 bond content [25]. Detailed examination of the Raman data with comparison to XPS data was described in a previous publication [16].

Variation in the deposition temperature led to a significant change in the surface morphology. Coatings deposited at 100–300 °C had a smooth surface with an average surface roughness (Ra) of about 0.8 nm (Fig. 8a and b). Further increases in the temperature led to a rapid increase in roughness (Fig. 8b–d). At 450 °C, the Ra exceeded 50 nm.

Surface energy is a very important characteristic to consider when examining the tribological properties of thin coatings. The wetting angle, which is characteristic of free surface energy [26], was about 90° and independent of deposition temperature (Fig. 9). This value is close to the characteristic value of diamond (93°) [27]. This observation shows that the surfaces of coatings deposited at all temperatures are saturated by sp^3 bonds and the saturation rate is not dependent on the kind of nanostructure—amorphous, nano-composite or nano-graphite. It could be noted, that variation of surface roughness affected on the measured wetting angle. Analysis of related references [28,29] shows that effect of roughness depends on a ratio between drop size and height of surface asperities. However, it could be assumed that the surface roughness of 50 nm did not effect significantly on the wetting angle due to the fact that this value was relatively low compare to size of drops used.

3.2. Mechanical properties and tribological behavior

The nano-hardness (H) and H/E ratio of the coatings are shown as a function of deposition temperature in Fig. 10. Analysis of the mechanical properties showed that the H/E ratio as well as nano-hardness had a maximum values in the region of nano-composite structures. The H/E ratio increased when the structure changed from amorphous to nano-composite to nano-graphite state in accordance with the growth of the fraction of the nano-graphite phase in the coatings. The H/E ratio reached its maximum when the nano-graphite was transformed to a nano-composite. A further increase in the deposition temperature within the nano-graphite region resulted in the monotonic decay of the H/E ratio and nano-hardness. The films deposited at *Ts* ~300 °C had the same nano-hardness as other DLC coatings [24,13].

Structural variation with an increase in the deposition temperature led to the formation of compressive stress in the coatings [16]. The presence of compressive stress is typical for DLC coatings, but the values vary in the range of 0.1 GPa [30,31] to 6 GPa [11] and exceed 10 GPa for coatings deposited by a cathodic arc method [32]. The stress level usually depends on the

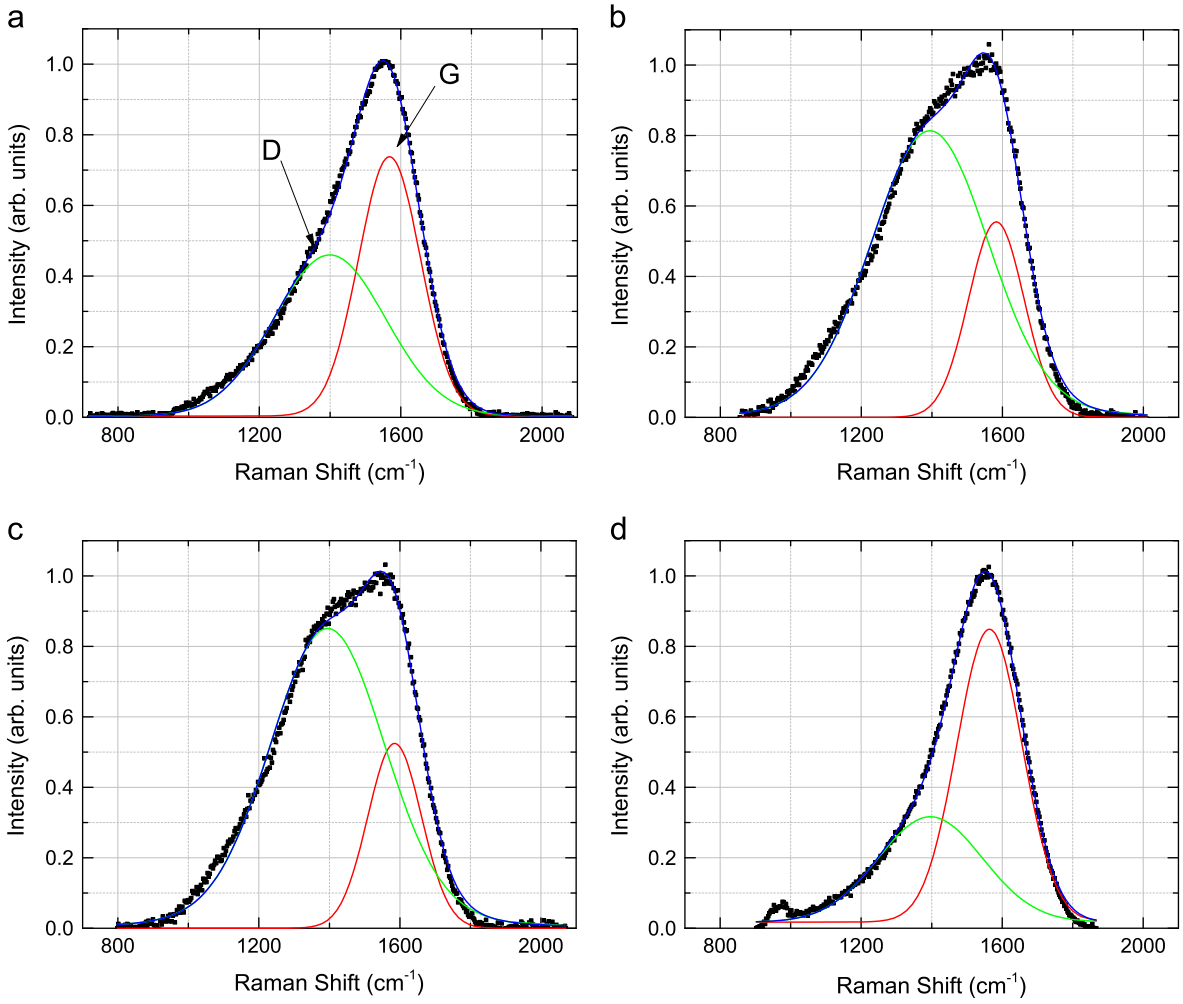

Fig. 7. Deconvolution of Raman spectra for coatings deposited at (a) 100 °C, (b) 200 °C, (c) 300 °C and (d) 450 °C.

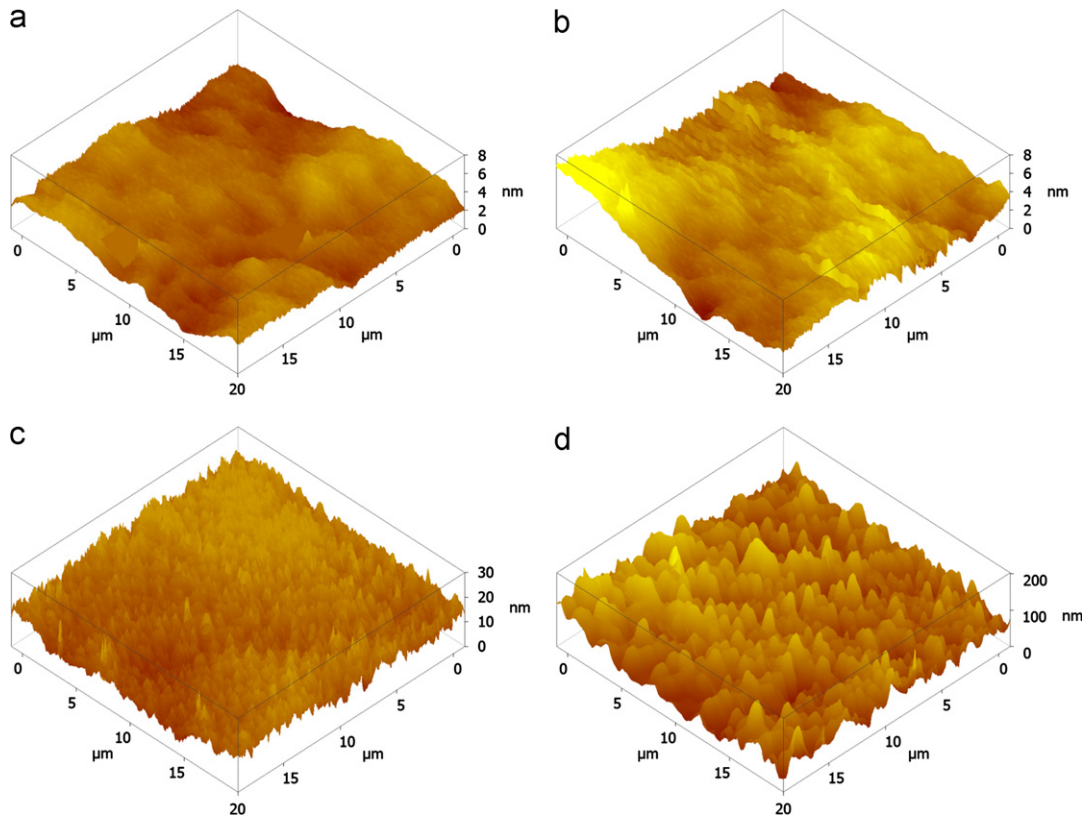

Fig. 8. AFM 3-D profile of coatings deposited at various deposition temperatures: (a) 100 °C, (b) 300 °C, (c) 400 °C and (d) 450 °C.

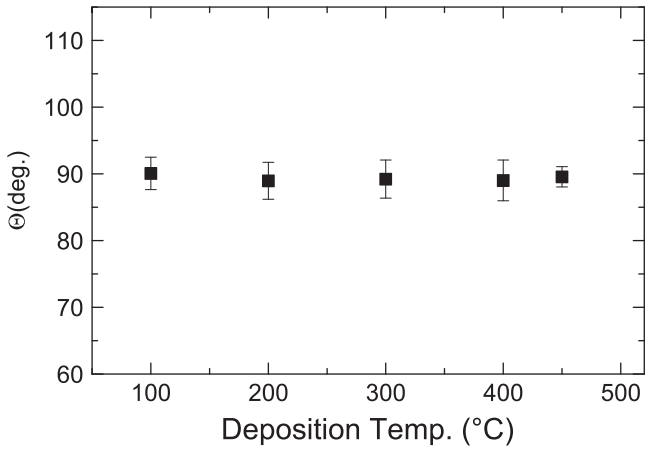

Fig. 9. Wetting angle of carbon nano-composite coatings as a function of deposition temperature.

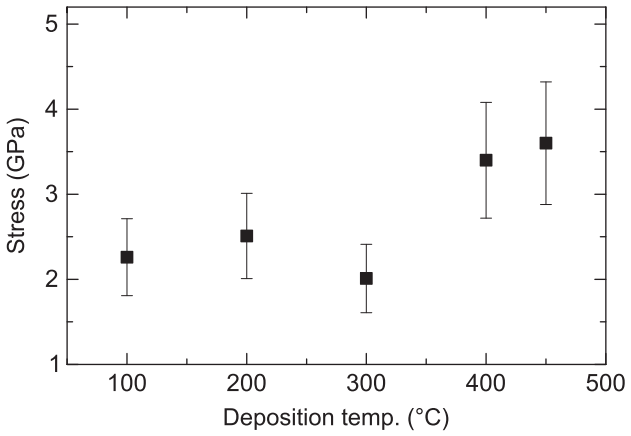

Fig. 11. Compressive stress in the coatings as a function of deposition temperature.

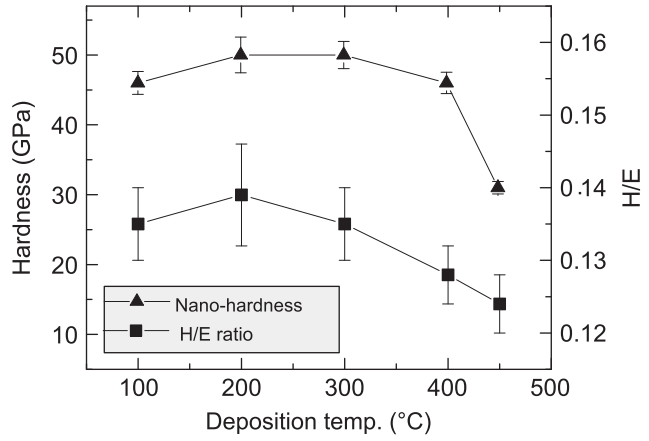

Fig. 10. Nano-hardness and H/E ratio as a function of deposition temperature.

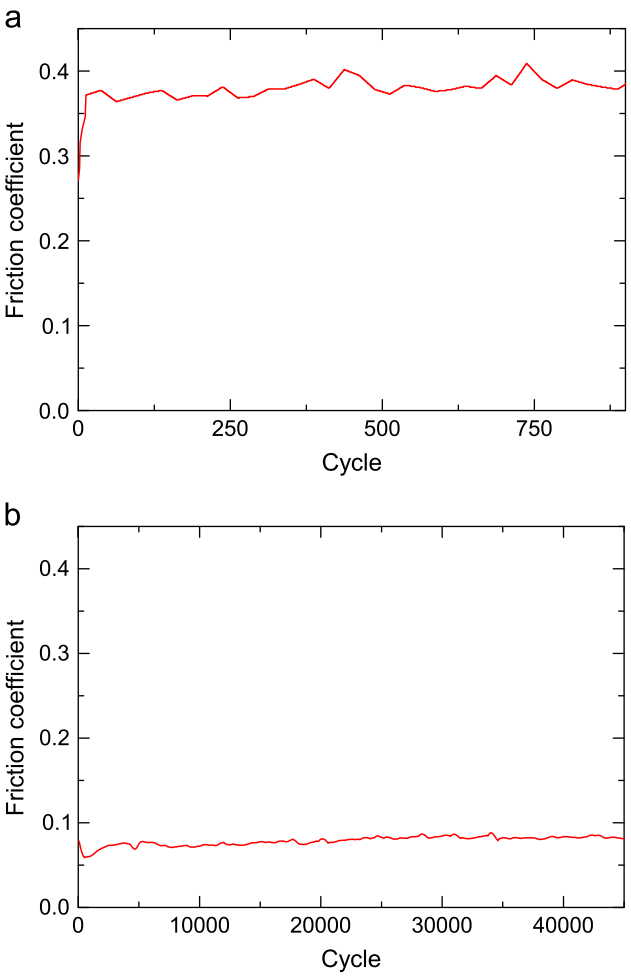

Fig. 12. Friction coefficient with respect to sliding cycles for coatings deposited at (a) 450 °C and (b) 300 °C.

deposition method and parameters. However, it was found that the stress level did not depend on the thickness of the coating in the range of 0.1–1 μm [33]. Values of compressive stress, calculated using Eq. (1) as function of the deposition temperature, are shown in Fig. 11. The relationship was non-linear. Two deviations are evident in this graph: moderate growth of the stress at 200 °C and further fall-back, and rapid growth at temperatures higher than 400 °C. Undoubtedly, this behavior was induced by changes in the nanostructure of the coatings described in the previous paragraph. Compared to previously published data, the observed stress level is moderate.

Tribological tests of the coatings films were conducted using a reciprocating pin-on-disk tribo-tester. Fig. 12 shows the average friction coefficient (COF) after three repeated tests for coatings deposited at 300 and 450 °C. At the higher deposition temperature (Fig. 12a), the COF increased from an initial value of about 0.3 to a steady-state value of ~0.38. Decreasing the deposition temperature down to 300 °C changed the frictional behavior of the film dramatically. The COF varied only slightly from 0.06 to 0.08 during the first 50 cycles and then reached a steady state at approximately 0.08 (Fig. 12b) and remained stable over a period of 45,000 cycles. This is a relatively low value compared to previously published data regarding the dry friction of DLC coatings under ambient conditions [12,24]. Fig. 13a shows the steady-state friction coefficient as a function of deposition temperature. For deposition temperatures in the range of 100°–300°, the coatings demonstrated low friction coefficient values of 0.08–0.1. A small increase in the friction coefficient was noted at 200 °C, but it subsequently decreased at 300 °C. When the temperature exceeded 400 °C, a rapid increase in the friction coefficient up to 0.38 was observed.

The wear rate was also dependent on the deposition temperature (Fig. 13b), but the scale of change was significantly higher. Starting from 0.04 μm^3/cycle in the range of 100–300 °C,

the wear rate showed significant increase at higher temperatures. At 450 °C, the wear rate was about three orders of magnitude higher compared to that at 300 °C. Thus, the wear behavior of the coatings deposited at temperatures above and below 400 °C was dramatically different. Fig. 14 shows SEM images of the wear tracks for coatings deposited at 300 and 450 °C. The duration of the wear test was 45,000 and 300 cycles, respectively. Coatings deposited at temperatures below 400 °C demonstrated very low wear (Fig. 14a), and a smooth, shallow wear track formed. The depth of the wear track in the central part was about 60 nm with a width of about 40 μm. The roughness inside of the wear track after wear tests was measured using an AFM. For the coating deposited at 300 °C the roughness was similar to the initial value of 0.8 nm, whereas the roughness inside of the wear track of the coating deposited at 450 °C increased significantly to 0.8 μm from the initial value of about 50 nm. Debris was located mostly at the end of the track, but some debris was also observed along the wear track. Debris located at the side were shifted from the edge of the wear track to a distance of about 10 μm, which could be due to the minor elastic deformation of the coating under the contact region. EDS analysis showed that the debris consisted of carbon. Furthermore, the counter surface material was not found in the debris or on the wear track. The wear increased significantly at higher deposition temperatures, and the coating was totally removed after only 300 cycles.

Wear of the counter surface was examined by SEM. However, no significant wear or transfer of the coating material was found. This was attributed to the high hardness and good chemical stability of the silicon nitride ball.

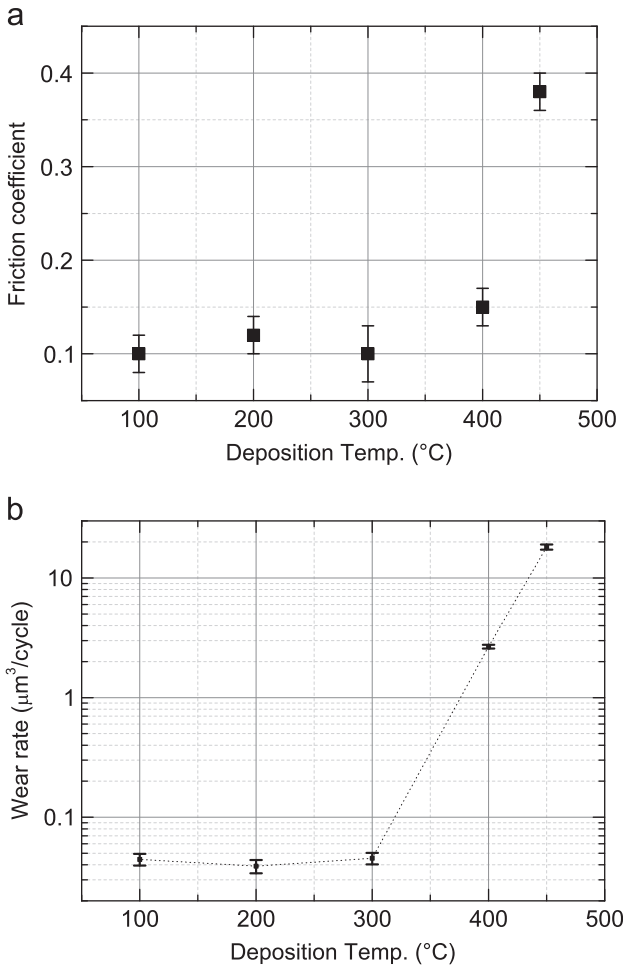

Fig. 13. Variation in (a) steady-state friction coefficient and (b) wear rate as a function of deposition temperature.

3.3. Discussion

The friction coefficient and wear of carbon coatings deposited using a C_{60} ion beam were unchanged and remained low at deposition temperatures below 400 °C. Explanations for this uncommon behavior were derived from peculiarities in the nanostructure of the coatings. Analysis of the TEM and SAED data showed that the coatings had a nano-composite structure when the deposition temperature exceeded 200 °C. At this temperature, reflections of graphite crystallites appeared in the SAED patterns (Fig. 3c). In the nano-composite coatings, nanocrystals of graphite were embedded into an amorphous diamond-like matrix. These graphite crystals were preferentially oriented and their graphene planes were perpendicular to the surface. The Young's modulus in the direction of the graphene plane was dictated primarily by sp^2 bonds and had a value of 1060 GPa. Along the direction normal to the graphene planes, Young's modulus was dictated primarily by van der Waals bonds and had a value of 36.5 GPa [34]. During the wear tests, the surface of friction was perpendicular to the graphene plates, and it was presumed that elastic deformation instead of destruction of the graphene planes took place during movement of the counter surface because their bond strength was higher than that of the diamond-like matrix [35]. Furthermore, shear deformation did not occur along the graphene planes. In contrast, the possibility of elastic deformation in the direction of a low Young's modulus (normal to the graphene planes) led to high H/E ratio values.

Nano-composite coatings had a relatively low level of compressive stress (2–2.5 GPa), which had a minimum at a deposition temperature of 300 °C. The non-monotonic effect of the deposition temperature on the stress level was due to the collision between C_{60} ions and the surface of the coating during its growth. It could be assumed that the compressive stress was low if relatively small (0.7–1 nm) nanocrystals formed as a result of the impact of C_{60} ions. Nanocrystals were formed below the surface due to the matter brought by the C_{60} ions, and the diamond-like phase formed on the

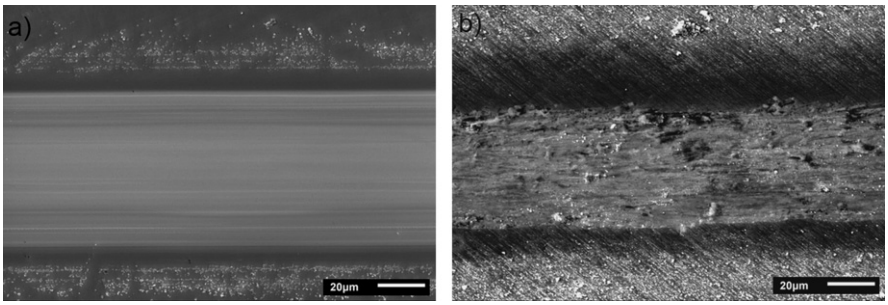

Fig. 14. SEM images of the wear track for coatings deposited at (a) 300 °C and (b) 450 °C after 45,000 and 300 cycles, respectively.

surface due to fast cooling. The stress was partially relaxed because the matter expanded in the direction of the free surface and the interplanar spacing of the graphite phase decreased. An increase in the deposition temperature led to transformation of the deeply located diamond-like phase into graphene layers under subsequent ion bombardment. Graphite crystals had a higher specific volume that led to an increase in the compressive stress. Therefore, the growth observed in this experiment is analogous to the subplantation model of growth [36], which is specific to DLC coatings. This model assumes that, instead of implantation of carbon atoms after impact by fullerene ions, the growth and coarsening of graphite crystals into the depth of the coatings takes place at elevated deposition temperatures. The growth of the graphite nanocrystals led to the thinning of the diamond-like matrix, a decrease in Young's modulus and hardness, and an increase in the surface roughness. All of these factors caused the wear rate to increase by several orders of magnitude in the wear experiment. Model of the structure of composite coating deposited by C60 ion beam and the mechanism of formation of interphase stress were described in detail in previous publications [15,16].

Absorption of water also plays an important role in the tribological properties of carbon coatings [34,37,38] by reducing the adhesive forces between friction surfaces. Water molecules present on the carbon surface can passivate the broken σ bonds and decrease the π–π^* interaction of graphite-like areas of the coating considerably. A wetting angle of 90° was characteristic of carbon coatings deposited using a C_{60} ion beam and corresponded to their nano-composite structure. Coatings with a nano-composite structure had a surface that consisted of graphite nanocrystals with diamond-like interlayers between them. Due to their preferential orientation, the more chemically active edges of the graphite layers outcrop onto the surface [39]. These edges had oriented terminal σ bonds (covalent bond interactions between unoccupied or dangling $sp^2\sigma$-bonds). These σ bonds were very active and easily produced surface oxides [34], and they could be passivated in atmosphere in the presence of water vapor through the formation of hydroxylic (−OH), carboxylic (−COOH), carbonylic (>C=O) or etheric (→C–O–C←) functional groups [40]. Subsequently, the surfaces interacted through hydrogen bonding of the hydroxyl groups during the frictional interaction. In addition, at high humidity, the formation of water nanodrops was possible [41], and these drops could play the role of a liquid lubricant.

These findings indicate that the low friction and wear properties of the coating deposited at a temperature of 300 °C could be explained not only by the mechanical and structural properties of the coatings, but also by the nano-structure of the surface. At higher deposition temperatures, both mechanical properties and surface morphology of the coatings were altered. Presence of high asperities on the surface increased the probability of wear due to interference of the asperities and increase in the abrasive action during the wear tests. This led to relatively high wear of the coatings deposited at high temperatures. Thus, at deposition temperatures above 300 °C, the benefit of the passivation layer formed on the surface in maintaining low friction could not be realized due to severe wear.

4. Conclusions

The effect of deposition temperature on the structure and tribological behavior of carbon nano-composite coatings deposited on a silicon substrate using an ion gun was assessed. Tribological tests were performed using a reciprocating tribotester under an applied load of 400 mN with a 1-mm-diameter silicon nitride ball used as the pin under ambient conditions. The following conclusions can be drawn from the experimental results:

1. Nano-composite carbon coatings demonstrate excellent tribological properties under ambient conditions. The friction coefficient was 0.08 and the wear rate was 0.04 μm^3/cycle.
2. The superior tribological properties of the coatings could be attributed to features of the nanostructure. The formation of preferentially-oriented graphite nanocrystals embedded in a diamond-like matrix led to an increase in the hardness and H/E ratio.
3. Deposition temperature significantly affects the nanostructure of the coating, surface morphology and mechanical properties. Deposition temperatures exceeding 400 °C led to the formation of a graphite phase and deteriorated the tribological characteristics of the coatings.

Acknowledgments

This work was supported by a National Research Foundation of Korea (NRF) grant funded by the Korean government (MEST) (No. 2012-0001232).

References

[1] Woo Y, Kim SH. Sensitivity analysis of plating conditions on mechanical properties of thin film for MEMS applications. Journal of Mechanical Science and Technology 2011;25:1017–22.
[2] Kim HJ, Kim DE. Nano-scale friction: a review. International Journal of Precision Engineering and Manufacturing 2009;10:141–51.
[3] Miyake S, Kaneko R. Microtribological properties and potential applications of hard, lubricating coatings. Thin Solid Films 1992;212:256–61.
[4] Kim DE, Kim CL, Kim HJ. A novel approach to wear reduction of micro-components by synthesis of carbon nanotube-silver composite coating. CIRP Annals—Manufacturing Technology 2011;60:599–602.
[5] Sung IH, Kim DE. Surface damage characteristics of self-assembled monolayers of alkanethiols on metal surfaces. Tribology Letters 2004;17:835–44.
[6] Donnet C, Ali Erdemir A. Tribology of diamond-like carbon films. Fundamentals and applications. NY: Springer US; 2008.
[7] Sharma N, Kumar N, Dhara S, Dash S, Bahuguna A, Kamruddin M, et al. Tribological properties of ultra nanocrystalline diamond film-effect of sliding counterbodies. Tribology International 2012;53:167–78.
[8] Voevodin A, Schneider J, Rebholz C, Matthews A. Multilayer composite ceramicmetal-DLC coatings for sliding wear applications. Tribology International 1996;29:559–70.
[9] Gayathri S, Kumar N, Krishnan R, Ravindran T, Dash S, Tyagi A, et al. Tribological properties of pulsed laser deposited DLC/TM (TM=Cr, Ag, Ti and Ni) multilayers. Tribology International 2012;53:87–97.
[10] Robertson J. Diamond-like amorphous carbon. Materials Science and Engineering R 2002;37:129–281.
[11] Deng J, Braun M. Residual stress and microhardness of DLC multilayer coatings. Diamond and Related Materials 1996;5:478–82.
[12] Tanaka A, Nishibori T, Suzuki M, Maekawa K. Tribological properties of DLC films deposited using various precursors under different humidity conditions. Diamond and Related Materials 2003;12:2066–71.
[13] Sedlacek M, Podgornik B, Vizintin J. Tribological properties of DLC coatings and comparison with test results: Development of a database. Materials Characterization 2008;59:151–61.
[14] Gaber H, Busmann HG, Hiss R, Hertel IV, Romberg H, Fink J, et al. Carbon films of amorphous and oriented graphitic structure from fullerene ion beam deposition. Journal of Physical Chemistry 1993;97:8244–9.
[15] Pukha V, Stetsenko A, Dub S, Lee J. Nanocrystalline diamond thin films deposited from C_{60} monoenergetic fullerene ion beam. Journal of Nanoscience and Nanotechnology 2007;7:1370–6.
[16] Pukha VE, Zubarev EN, Drozdov AN, Pugachov AT, Jeong SH, Nam SC. Growth of nanocomposite films from accelerated C_{60} ions. Journal of Physics D 2012;45:335302–9.
[17] Ionov N. Study of gas-discharge and cosmic plasmas by means of multi-electrode probes - a review. Zhurnal Tekhnicheskoi Fiziki 1964;34:591–610.
[18] Ohring M. Materials science of thin films. 2nd ed. San Diego: Academic Press; 2002.
[19] Wilcock J, Campbell D. A sensitive bending beam apparatus for measuring the stress in evaporated thin films. Thin Solid Films 1969;3:3–12.
[20] Hopcroft M, Nix W, Kenny T. What is the Young's modulus of silicon? Journal of Microelectromechanical Systems 2010;19:229–38.
[21] Johnson KL. Contact mechanics. Cambridge: Cambridge University Press; 1985.

[22] Dawson JC, Adkins CJ. Conduction mechanisms in amorphous carbon prepared by ion-beam sputtering. Journal of Physics: Condensed Matter 1995;7:6297–315.
[23] Pukha V, Pugachov A, Churakova N, Zubarev E, Vinogradov V, Nam S. Synthesis, structure and properties of superhard nanostructured films deposited by the C_{60} ion beam. Journal of Nanoscience and Nanotechnology 2012;12:4762–8.
[24] Lusk D, Gore M, Boardman W, Casserly T, Boinapally K, Oppus M, et al. Thick DLC films deposited by PECVD on the internal surface of cylindrical substrates. Diamond and Related Materials 2008;17:1613–21.
[25] Kataria S, Dhara S, Barshilia HC, Dash S, Tyagi AK. Evolution of coefficient of friction with deposition temperature in diamond like carbon thin films. Journal of Applied Physics 2012;112:023525–8.
[26] Lugscheider E, Bobzin K. The influence on surface free energy of PVD-coatings. Surface and Coatings Technology 2001;142–144:755–60.
[27] Ostrovskaya L, Ralchenko V, Bolshakov A, Saveliev A, Dzbanovsky N, Shmegera S. Wettability of ultrananocrystalline diamond and graphite nanowalls films: a comparison with their single crystal analogs. Journal of Nanoscience and Nanotechnology 2009;9:3665–71.
[28] Miwa M, Nakajima A, Fujishima A, Hashimoto K, Watanabe T. Effects of the Surface Roughness on Sliding Angles of Water Droplets on Superhydrophobic Surfaces. Langmuir 2000;16:5754–60.
[29] Zhou B, De Hosson TM. Influence of surface roughness on the wetting angle. Journal of Materials Research 1995;10:1984–92.
[30] Oka Y, Kirinuki M, Nishimura Y, Azuma K, Fujiwara E, Yatsuzuka M. Measurement of residual stress in DLC films prepared by plasma-based ion implantation and deposition. Surface and Coatings Technology 2004;186:141–5.
[31] Morshed M, McNamara B, Cameron D, Hashmi M. Stress and adhesion in DLC coatings on 316L stainless steel deposited by a neutral beam source. Journal of Materials Processing Technology 2003;143–144:922–6.
[32] Lau DW, Partridge JG, Taylor MB, McCulloch DG, Wasyluk J, Perova TS, et al. Microstructural investigation supporting an abrupt stress induced transformation in amorphous carbon films. Journal of Applied Physics 2009;105:084302–6.
[33] Karaseov PA, Podsvirov OA, Karabeshkin KV, Vinogradov AY, Azarov AY, Karasev NN, et al. Influence of ion irradiation on internal residual stress in DLC films. Nuclear Instruments and Methods in Physics Research Section B 2010;268:3107–10.
[34] Pierson HO. Handbook of carbon, graphite, diamond, and fullerenes: properties, processing, and applications. Park Ridge NJ: Noyes; 1993.
[35] Zhang B, Guo W. Cracking diamond anvil cells by compressed nanographite sheets near the contact edge. Applied Physics Letters 2005;87 051907–3.
[36] Lifshitz Y, Lempert G, Grossman E, Avigal I, UzanSaguy C, Kalish R, et al. Growth mechanisms of DLC films from C+ ions: experimental studies. Diamond and Related Materials 1995;4:318–23.
[37] Erdemir A, Donnet C. Tribology of diamond-like carbon films: recent progress and future prospects. Journal of Physics D 2006;39:R311–27.
[38] Konicek AR, Grierson DS, Sumant AV, Friedmann TA, Sullivan JP, Gilbert PU, et al. Influence of surface passivation on the friction and wear behavior of ultrananocrystalline diamond and tetrahedral amorphous carbon thin films. Physical Review B 2012;85:155448.
[39] Panigrahi S, Bhattacharya A, Bandyopadhyay D, Grabowski SJ, Bhattacharyya D, Banerjee S. Wetting property of the edges of monoatomic step on graphite: frictional-force microscopy and ab initio quantum chemical studies. Journal of Physical Chemistry C 2011;115:14819–26.
[40] Boehm H. Surface oxides on carbon and their analysis: a critical assessment. Carbon 2002;40:145–9.
[41] Cao P, Xu K, Varghese JO, Heath JR. The microscopic structure of adsorbed water on hydrophobic surfaces under ambient conditions. Nano Letters 2011;11:5581–6.